



RESEARCH ARTICLE | MAY 05 2022

# Research on the electric life evaluation technology of the arc extinguishing chamber of the 550 kV circuit breaker

Xiaopo Mao  ; Yaodong Zhang; Suge Tu; Bin Xiang



AIP Advances 12, 055212 (2022)

<https://doi.org/10.1063/5.0084883>



CrossMark

## Articles You May Be Interested In

Analysis of contact ablation of circuit breaker after short circuit current breaking

*AIP Advances* (October 2023)

Simulation study on arc motion process of DC miniature circuit breakers

*AIP Advances* (October 2023)

Simulation study of influence of the outlet elastic baffle on pressure in arc chamber during the interrupting process of low-voltage circuit breaker

*AIP Advances* (June 2021)

26 October 2023 18:04:00

## AIP Advances

Why Publish With Us?



**25 DAYS**  
average time  
to 1st decision



**740+ DOWNLOADS**  
average per article



**INCLUSIVE**  
scope

[Learn More](#)



# Research on the electric life evaluation technology of the arc extinguishing chamber of the 550 kV circuit breaker

Cite as: AIP Advances 12, 055212 (2022); doi: 10.1063/5.0084883

Submitted: 11 January 2022 • Accepted: 24 February 2022 •

Published Online: 5 May 2022



View Online



Export Citation



CrossMark

Xiaopo Mao,<sup>1,a)</sup>  Yaodong Zhang,<sup>1</sup> Suge Tu,<sup>2</sup> and Bin Xiang<sup>1</sup>

## AFFILIATIONS

<sup>1</sup> State Grid Hubei Electric Power Co., Ltd., Electric Power Research Institute, Wuhan, Hubei 430077, China

<sup>2</sup> State Grid Hubei Transmission and Transformation Engineering Co., Ltd., Wuhan, Hubei 430077, China

<sup>a)</sup> Author to whom correspondence should be addressed: mxp2004@163.com

## ABSTRACT

When the circuit breaker is switched on and off, the phenomenon of arc ablation will occur. Under the action of the electric arc, the surface of the contact is constantly damaged, resulting in deformation and material evaporation. With the increase in the electric arc temperature, the material loss on the contact surface of the circuit breaker increases. In this paper, according to the three major factors affecting the electrical life of the circuit breaker arc extinguishing chamber—the state of the arc contact, the nozzle, and the SF<sub>6</sub> gas—the corresponding test detection methods and evaluation methods are proposed. With the continuous accumulation of the breaking current, the effective contact displacement between the arc contacts decreases and the average contact resistance increases. The effective contact displacement decreases exponentially with the increase in the cumulative breaking energy. The content of CF<sub>4</sub> can be used not only to characterize the discharge ablation on the surface of the nozzle insulating material but also to characterize the discharge decomposition degree of SF<sub>6</sub> in the system by adding carbonaceous compounds. Through the experiment, it is suggested that CF<sub>4</sub> should reach 600 μl/l as the threshold for judging whether the arc extinguishing chamber needs maintenance. This method can be extended to the working condition evaluation of the arc extinguishing chamber of other types of the SF<sub>6</sub> circuit breaker.

© 2022 Author(s). All article content, except where otherwise noted, is licensed under a Creative Commons Attribution (CC BY) license (<http://creativecommons.org/licenses/by/4.0/>). <https://doi.org/10.1063/5.0084883>

## I. INTRODUCTION

The operating state of a circuit breaker is usually determined by its electrical life. During the operation of the power system, when the circuit breaker is opened and closed frequently and the number of circuit breakers reaches the upper limit, it is necessary to carry out maintenance work for the circuit breaker and analyze the loss of the contacts.<sup>1,2</sup> At the same time, there are also requirements in the system countermeasures, and it is necessary to check whether the breaking short-circuit current capacity of the circuit breaker itself meets the requirements of operation. For the circuit breaker with multiple breaking short-circuit current, it is necessary to evaluate its cumulative effect on the electrical performance of the arc extinguishing chamber.<sup>3,4</sup>

At present, the scale of the power system is increasing, and the system impedance is decreasing. If a short-circuit fault occurs, the

impact of the short-circuit current on the power grid will increase. The cumulative effect of the short-circuit current on the circuit breaker should not be underestimated. Among them, a large number of AC filters are put into use in the power system. Due to the change in the power grid load, the working state of the circuit breaker is constantly changed. In particular, the capacitive load in the system reduces the service life of the arc contact of the arc extinguishing chamber.<sup>5,6</sup>

In order to reflect the breaking level of the circuit breaker, under the condition of rated short-circuit current, it is used to measure the electrical life of the circuit breaker according to the number of times the circuit breaker can be switched. When the circuit breaker performs the switching operation, the phenomenon of arc ablation will occur. Under the action of the electric arc, the surface of the contact is continuously damaged, which is called electrical wear. The main factors affecting electrical wear are the structure of

the arc extinguishing chamber, the switching current, the switching speed, and the arc duration.<sup>7,8</sup>

At present, there are mainly four non-disintegrated evaluation methods for the contact state of the circuit breaker arc extinguishing chamber, namely: (1) static resistance measurement method; (2)  $N-I_b$  life curve analysis technology; (3) contact overtravel time modeling technology; and (4) dynamic resistance measurement method. The cumulative effect of the short-circuit current of the circuit breaker opening and closing is mainly reflected in whether the contacts and nozzles in the arc extinguishing chamber are ablated by abnormal arcs and the mechanical wear of the contacts under high-temperature arcs. Therefore, this paper focuses on the evaluation of the residual capacity of the arc extinguishing chamber to break the fault current and then quantitatively estimate the residual electrical life of the circuit breaker, which provides a theoretical basis for the subsequent operation and maintenance. Based on the above purpose, this paper proposes the corresponding test detection methods and evaluation methods for the three major factors affecting the electrical life of the circuit breaker arc extinguishing chamber, namely, the state of the arc contacts, the nozzles, and the SF<sub>6</sub> gas.<sup>9</sup>

## II. TEST PROTOTYPE AND ITS MATERIAL SELECTION

The test prototype used in this paper is a circuit breaker with a CYA4 hydraulic spring operating mechanism. The specific model is the LW15-550 porcelain column circuit breaker with a voltage level of 500 kV, and the maximum operating voltage is 550 kV. The main contact selection mode is copper silver-plated alloy, and the arc contact adopts CuW<sub>70</sub> alloy, as shown in Fig. 1. In Fig. 1, 1 is the wiring board, 2 is the terminal, 3 is the static contact base, 4 is the contact between the moving contact and the static contact, 5 is the contact point between the nozzle base and the pressure cylinder, 6 is the contact point between the moving contact and the pressure cylinder, 7 is the pressure cylinder, 8 is the contact point between the intermediate contact and the pressure cylinder, 9 is the intermediate contact, 10 is the support member, and 11 is the body shell.

Table I shows the materials used for some parts of the circuit breaker. Since the arc generated during the switching process of the circuit breaker will ablate the surface material, resulting in the electrical wear of the material. The surface material of the circuit breaker needs to go through three periods in total, which are the aging period, the stable period, and the failure period. The most critical period affecting the performance of the surface materials is the stable period. When the ratio of Cu element and W element in the material is reasonable, the stable period of surface material operation can be increased.

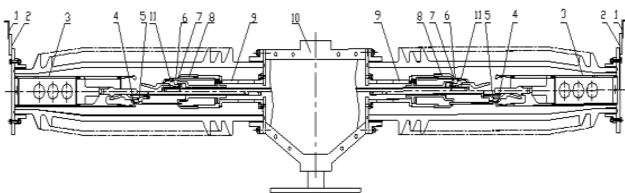


FIG. 1. Schematic diagram of the arc extinguishing chamber of the test prototype.

TABLE I. Key component parameters of the arc extinguishing chamber of the test prototype.

Part	Material
Nozzle	PTFE F4 + 7%BN $\phi 35/\phi 110 \times 190$
Moving contact	$\Phi 170 \times 17.5$ chrome bronze tube QCr <sub>0.5</sub>
Static contact	$210 \times 30$ chrome bronze tube QCr <sub>0.5</sub>
Intermediate contact	Chrome bronze QCr <sub>0.5</sub>
Moving arc contact	Copper-tungsten alloy CuW <sub>70</sub> /chrome copper QCr <sub>0.5</sub>
Static arc contact	Copper-tungsten alloy CuW <sub>70</sub> /chrome copper QCr <sub>0.5</sub>

## III. TEST RESEARCH ON CONTACT PERFORMANCE OF CIRCUIT BREAKER ARC CHAMBER

The motion state of the single-fracture arc extinguishing contact of the test prototype can be divided into four main key states, namely, the fully closed state, the just-separated state of the main contact, the just-separated state of the arc contact, and the fully opened state. The surface state and length change of the dynamic and static arc contacts can be determined by the dynamic resistance measurement method, as shown in Fig. 2. The basic principle is to measure the change in the contact resistance during the movement of the dynamic and static arc contacts by using the volt-ampere characteristics. The fracture model is separated at a certain speed. In the separation process, the contact resistance of the arc contact is measured and then supplemented by the mechanical characteristics of the action of the circuit breaker, the specific position of the dynamic and static arc contacts in the separation process can be obtained, and the effective contact resistance displacement can be calculated. The average resistance value within the effective displacement of the contact resistance characterizes the surface state of the arc contact, while the effective displacement characterizes the effective length of the arc contact. The variation of the

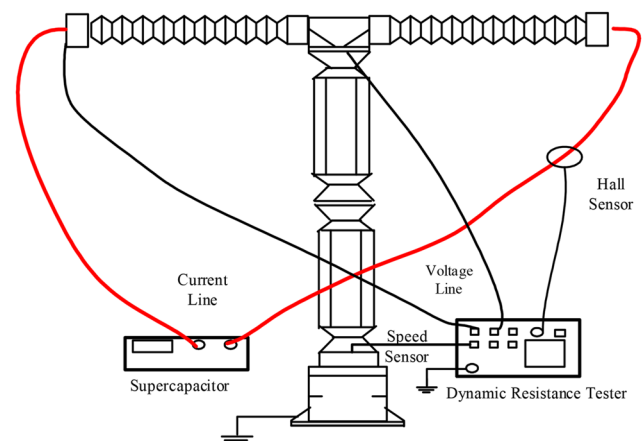


FIG. 2. Wiring diagram of the dynamic resistance tester.

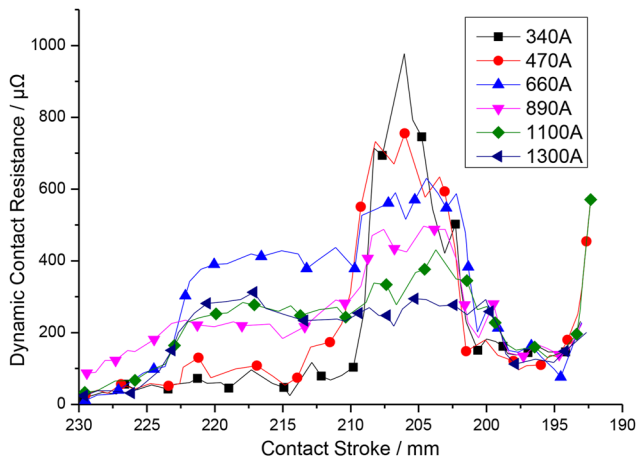


FIG. 3. The opening part of the dynamic contact resistance curve at different currents.

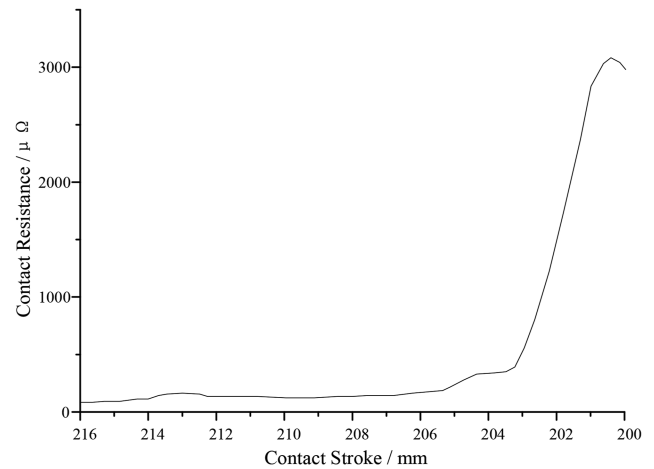


FIG. 4. The relationship between the contact stroke and contact resistance.

average resistance and the effective length before and after breaking will characterize the ablation of the arc contacts in the circuit breaker.

Compare the measured contact resistance under different test currents, as shown in Fig. 3. 230–220 mm corresponds to the copper–chromium segment of the static contact, 220–205 mm corresponds to the copper–tungsten segment, and 205 mm to the end about 192 mm corresponds to the chamfered part of the static contact rubbed by the moving contact finger. The internal contact plane of the moving contact finger is 12 mm long. As can be seen from Fig. 3, the greater the current, the more stable the dynamic contact resistance, the smaller the fluctuation, and the more accurate the calculation of the arc contact stroke. On the contrary, the smaller the current, the greater the fluctuation of the dynamic contact resistance, and the higher the peak value.

#### IV. STUDY ON THE TREND OF DYNAMIC RESISTANCE DURING THE ELECTRICAL LIFE TEST OF 500 kV CIRCUIT BREAKERS

With the increase in the test cumulative breaking current energy, the effective contact stroke of the arc contact is gradually shortened, the shorter the stable time of the contact resistance value within a certain threshold range, and the higher the average contact resistance value per unit stroke under the same stroke, as shown in Figs. 4 and 5.

With the continuous accumulation of breaking current, the effective contact displacement between the arc contacts decreases and the average contact resistance increases. In order to evaluate the cumulative effect of the breaking current, through experiments and comparative analysis, it is found that the effective contact displacement decreases exponentially with the increase in the cumulative breaking energy, as shown in Fig. 6. The corresponding relationship between the cumulative breaking energy, effective contact displacement, and average contact resistance is analyzed in the following.

Under the cumulative breaking energy  $Q$  ( $\sum I^2 \times 10^4$  kJ), the effective contact displacement of the arc contact is exponentially fitted, and the relationship between the effective contact displacement and the cumulative breaking energy can be obtained as follows:

$$L = 8.8 \times e^{\frac{-Q}{3.5}}. \tag{1}$$

The average contact resistance increases exponentially with the increase in the cumulative breaking energy. Figure 7 shows the trend distribution diagram of the average contact resistance.

Under the cumulative breaking energy  $Q$  ( $\sum I^2 \times 10^4$  kJ), the average contact resistance of the arc contact is exponentially fitted, and the relationship between the average contact resistance and the cumulative energy can be obtained as follows:

$$\bar{R} = \frac{Q}{3}. \tag{2}$$

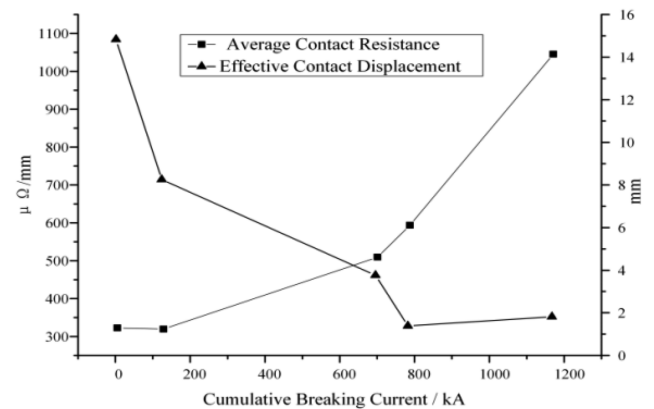


FIG. 5. The relationship between the contact displacement, resistance, and accumulated current of the fracture arc contact.

26 October 2023 18:04:00

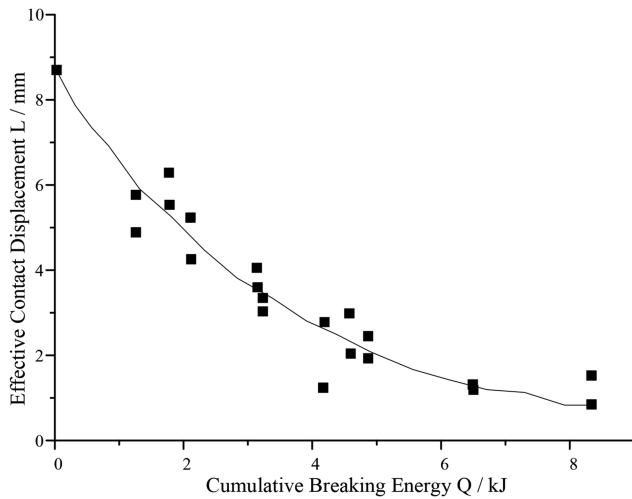


FIG. 6. Trend distribution diagram of effective contact displacement.

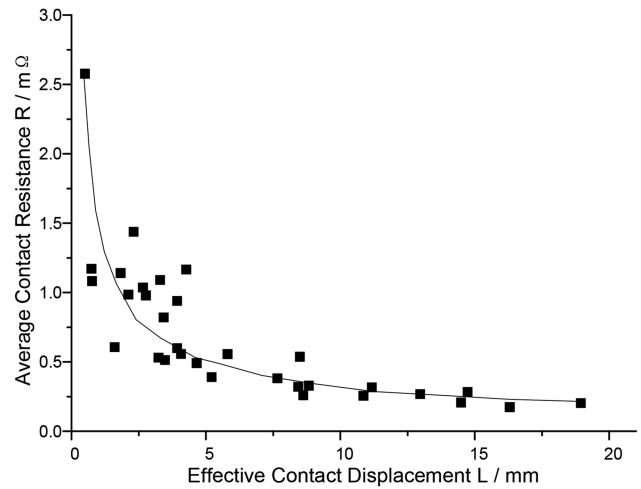


FIG. 8. Distribution of the average contact resistance with displacement.

When the effective contact displacement  $L$  is in the range of 0–5 mm, the average contact resistance decreases rapidly with the increase in the effective contact displacement. After the contact displacement is greater than 5 mm, the change of the average contact resistance tends to be stable, and the trend distribution diagram of the average contact resistance with the displacement is shown in Fig. 8.

The power function fitting is performed on the average contact resistance corresponding to the effective contact stroke of the arc contact, and the relationship formula between the average contact resistance and the effective contact displacement can be obtained as follows:

$$\bar{R} = 1.4 \times L^{-0.6}. \tag{3}$$

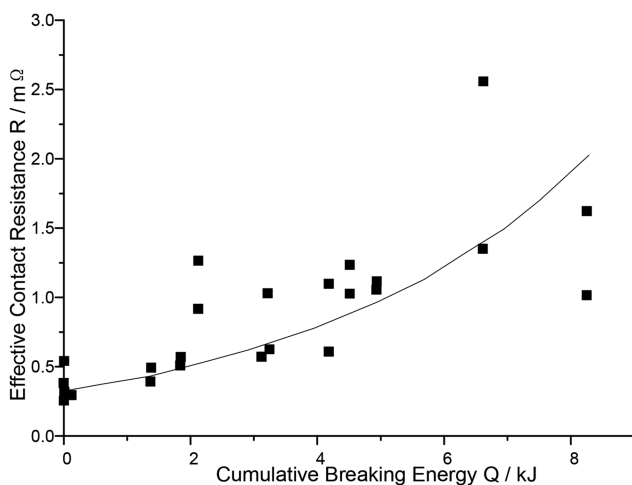


FIG. 7. Trend distribution graph of the average contact resistance.

According to the relationship between the contact mass loss of the prototype and the amplitude of the breaking short-circuit current, the contact mass erosion amount can be calculated. According to the arcing time and the current peak value, the coulomb quantity of each breaking test can be calculated. In practice, the current is an attenuation waveform, but the arcing time is fixed at 15 ms, which can be approximately calculated as

$$C = \int_0^t I_m \sin(2\pi ft) dt. \tag{4}$$

In formula (4),  $C$  is the coulomb quantity;  $t$  is the arcing time;  $I_m$  is the current peak value;  $f$  is the frequency.

The average mass loss per unit of coulomb is calculated as

$$F = \Delta m / \sum_1^{100} C. \tag{5}$$

### V. ANALYSIS OF THE ABLATION OF THE CONTACTS OF THE CIRCUIT BREAKER

In the process of contact opening and closing, it will experience repeated ablation and wear of the arc. After each ablation wear, the composition, performance, and shape of the contact surface are constantly changing. It leads to cracks, slag dropping, melting, evaporation, and other phenomena on the surface of the contact, which eventually leads to the failure of the contact, and the switch cannot be opened and closed normally. In order to study the failure mechanism of arc erosion after the arc contact breaks the short-circuit current, a pair of arc contacts with a cumulative breaking short-circuit current test are selected as the research object. The metallography and energy spectrum of the arc contact are analyzed, and the analysis results are compared with the new arc contact to reveal the evolution and development process of the arc contact from breaking and cumulative arc ablation to failure.



FIG. 9. Macromorphology of the contact surface.

TABLE II. Test items and equipment.

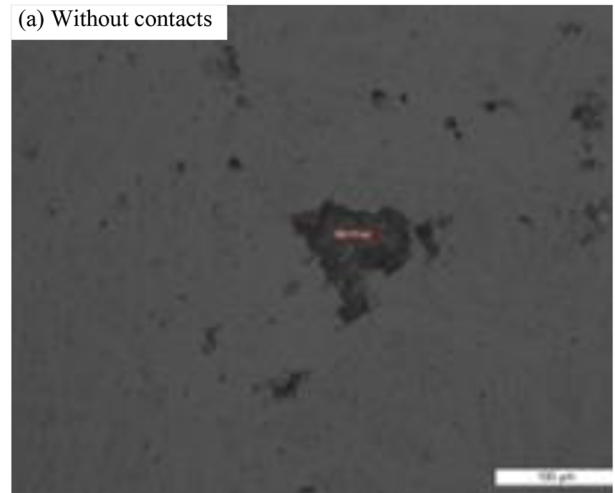
Equipment	Model
Leica metallurgical microscope	DMI3000M/325754
Electric refrigeration spectrometer	EDAX Apollo X

Macroscopically, after cumulative ablation, the contact is adhered and blackened by the ablation, as shown in Fig. 9. The surface of the static arc contact is generally cracked, uneven, with small holes, and the arc-shaped contact surface is flattened. The moving arc contact also shows certain cracking, but the crack depth is less than that of the static arc contact. Since the contact finger structure of the moving arc contact disperses the energy of arc ablation, the overall ablation degree of the moving arc contact is less serious than that of the static arc contacts. At the same time, the contact fingers are also deformed, and they become rounded and thinned in the process of the arc ablation and the opening and closing of the circuit breaker.

The test items include metallography and energy spectrum, as shown in Table II. The metallographic inspection of the circuit breaker contact mainly detects defects, such as inclusions, cracks, voids, and aggregates, in alloy samples.

It can be seen from Fig. 10 that compared with the metallographic structure without ablation, obvious cracks have been generated on the surface of the sampling point in the ablation center, which have spread from the surface to the inside, and the crack depth is close to about 500  $\mu\text{m}$ . In the process of multiple arcing, the copper melts and evaporates under the action of the arc, and microcracks begin to form on the surface. The tungsten particles on the surface are re-sintered under the action

(a) Without contacts



(b) Contact after ablation

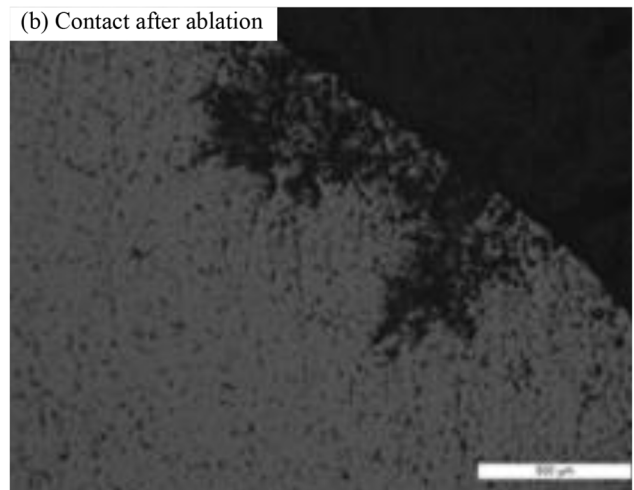


FIG. 10. Comparison of metallographic detection of contacts.

of a high temperature, resulting in cracks in the tungsten skeleton. Under the action of high-temperature arcs, the gas pressure increases sharply, which forms compressive stress on the cracks formed by ablation and promotes the inward expansion of the cracks. At the same time, the repeated opening and closing of the contacts causes the copper at the front of the crack to melt, volatilize, expand, solidify, and shrink repeatedly, which also leads to crack propagation.

TABLE III. Energy spectrum analysis results.

Sample	O (%)	F (%)	S (%)	W (%)	Other ingredients
Without ablation	7.11	0	0	78.8	C:0.63
After ablation	5.45	11.35	5.4	14.64	C:0.84, N:2.04, Fe:2.15, Al:7.15, K:0.88, and Ca:0.67

The results of the energy spectrum analysis are shown in Table III. It can be seen from Fig. 10 and Table III that there are obvious turtle cracks on the surface of the ablation center compared with the microscopic morphology without ablation. In the process of multiple opening and closing of the circuit breaker, melting and solidification occur alternately, and the middle part of the crack is continuously affected by the compression-tensile stress, which makes the crack propagate, and new cracks are generated in the process of the propagation, and the crack-like cracks are finally formed after repeated operations. The bulging and unevenness on the surface are aggravated, and the bulging is formed by the repeated vaporization and deposition of Cu in the alloy during the ablation process. There are trace amounts of Fe and Al in the energy spectrum, which are mainly derived from the cast iron material of the contact base and a small amount of nozzle alumina filler.

## VI. RESEARCH ON GAS COMPOSITION TREND OF CIRCUIT BREAKER SWITCHING CURRENT TEST

The opening and closing current test of the LW15A-550 circuit breaker is used to track and analyze the change trend of the SF<sub>6</sub> gas composition. Through timed quantitative detection and analysis, the circuit breaker closes and breaks currents of different energy, resulting in the change trend of the gas component, so as to extract the key characteristic components of the gas components. Combined with the dynamic resistance test method, the performance status of the current circuit breaker arc extinguishing chamber is evaluated from different dimensions. The contents of H<sub>2</sub>, air, CO, CO<sub>2</sub>, CH<sub>4</sub>, CF<sub>4</sub>, C<sub>2</sub>F<sub>6</sub>, C<sub>3</sub>F<sub>8</sub>, H<sub>2</sub>S, SO<sub>2</sub>, SOF<sub>2</sub>, SO<sub>2</sub>F<sub>2</sub>, COS, and CS<sub>2</sub> and other impurity components in the SF<sub>6</sub> gas were detected by helium ion gas chromatography. According to the requirements of the on-site remote and continuous test, the component analysis test is carried out in the way of host-wireless routing-panel control acquisition, as shown in Fig. 11.

In the two experiments in July and November, the change trend of some components of 120 closing tests of the circuit breaker is shown in Fig. 12. In the two experiments, the final decomposition concentration comparison after 120 closing tests of the circuit breaker is shown in Table IV.

Comparing the test data of the two experiments (where July represents the first round of experiment and November represents the second round of experiment), it can be found that:

- (1) The variation trends of air and CF<sub>4</sub> components in the experiment in November were similar to those in the experiment in July. The decline in November should be related to the temporary addition of new gas. If new gas is not added, the trend should be gradual growth.



FIG. 11. Composition diagram of the component test system.

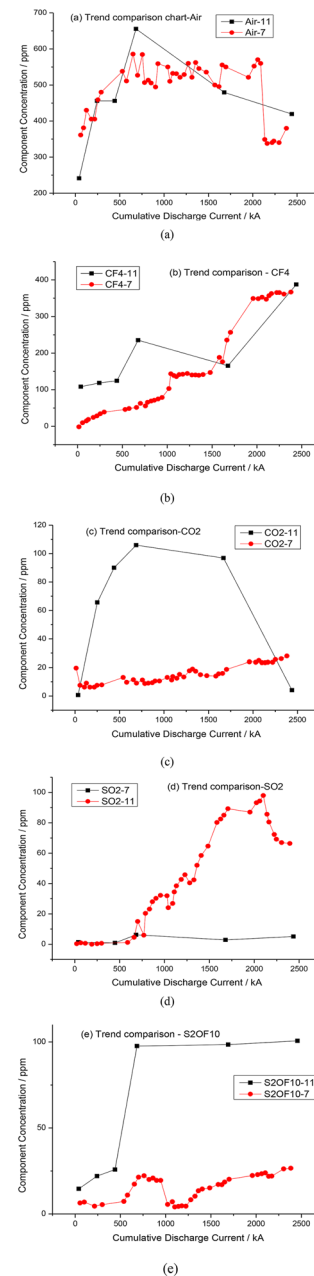


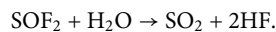
FIG. 12. The changing trend of some components of the 120 closure tests in two experiments (July and November). (a) Trend comparison chart—Air. (b) Trend comparison—CF<sub>4</sub>. (c) Trend comparison—CO<sub>2</sub>. (d) Trend comparison—SO<sub>2</sub>. (e) Trend comparison—S<sub>2</sub>OF<sub>10</sub>.

- (2) The variation trends of CO and CO<sub>2</sub> components are quite different. In the experiment in November, the CO<sub>2</sub> content first gradually increased, and then, the content of both decreased at the end of the experiment.
- (3) The obvious difference between the two experiments is the difference in the content of SOF<sub>2</sub> and SO<sub>2</sub>. The SO<sub>2</sub> content was significant and gradually increased in July, but the

**TABLE IV.** Comparison of data of the two experiments (July and November) (concentration/ppm).

Component	7–120 closing	7–10+ breaking	11–120 closing	11–10 breaking
Air	370.80	396.93	438.00	928.00
CF <sub>4</sub>	506.59	634.83	399.7	748.00
CO	2.5	36.6	14.9	5.6
CO <sub>2</sub>	42.32	56.23	5.80	15.39
SO <sub>2</sub>	64.00	75.39	5.10	12.61
SOF <sub>2</sub>	0.00	0.00	438.00	640.00
S <sub>2</sub> OF <sub>10</sub>	40.02	52.46	98.90	274.00
SO <sub>2</sub> F <sub>2</sub>	0	0	0	3.34
COS	1.22	5.62	0.00	0.00
H <sub>2</sub> S	0.51	1.74	0.00	1.18

SOF<sub>2</sub> component could not be detected. The experiment in November showed that there was a large amount of SOF<sub>2</sub>, while the concentration of SO<sub>2</sub> was very low and the change was not obvious. The difference is due to the difference in humidity within the gas chamber. When the micro-water content in the gas chamber is high, the reaction amount of SOF<sub>2</sub> and H<sub>2</sub>O is greater, and more SO<sub>2</sub> will inevitably be generated. The reaction equation is as follows:



In the experiment, the SOF<sub>2</sub> content is very high, and the SO<sub>2</sub> content is very little, which is due to the large difference in the micro-water content in the SF<sub>6</sub> gas chamber between the two experiments. It is found that in order to generate CF<sub>4</sub>, the continuous reaction of CH<sub>x</sub> with F and HF molecules must be carried out to generate CF<sub>3</sub> radicals and then react with F atoms or SF<sub>x</sub> to generate CF<sub>4</sub>. For the C sources starting from insulating materials, this is the only way to generate CH<sub>4</sub>.

Theoretically, CF<sub>4</sub> is transformed from the nozzle material by high-energy particle radiation. The greater the amount of CF<sub>4</sub> generated, the greater the loss of PTFE, and the larger the throat diameter of the nozzle. During the opening process of the circuit breaker, the gas pressure of SF<sub>6</sub> acting on the throat of the nozzle will drop, which will affect the rise rate of the insulation of the arc extinguishing chamber after arcing. However, the small capacitive current itself has a relatively slight burning effect on the copper–tungsten alloy contacts. Therefore, under this working condition, the change in the nozzle shape will affect the success of the breaking.

In summary, the content of CF<sub>4</sub> can not only be used to characterize the ablation discharge on the surface of the nozzle insulating material, but can also characterize the discharge decomposition degree of SF<sub>6</sub> in the system by adding carbonaceous compounds. Through experiments, it is recommended that CF<sub>4</sub> should reach 600 μl/l as the threshold for judging whether the arc extinguishing chamber needs to be repaired. This method can be extended to the operating condition evaluation of the arc extinguishing chamber of other types of the SF<sub>6</sub> circuit breaker.

## VII. CONCLUSION

In this paper, the LW15-550 type column circuit breaker is used as the test prototype, and the CuW<sub>70</sub> arc contact is used to carry out the relevant experimental research on the electrical life of the arc extinguishing chamber of the circuit breaker. The research results show the following:

- (1) The greater the current, the more stable the dynamic contact resistance, the smaller the fluctuation, and the more accurate the calculation of the arc contact stroke. On the contrary, the smaller the current, the greater the fluctuation of the dynamic contact resistance and the higher the peak value.
- (2) With the continuous accumulation of breaking current, the effective contact displacement between the arc contacts decreases and the average contact resistance increases. The effective contact displacement decreases exponentially with the increase in the cumulative breaking energy.
- (3) In the process of multiple arcing, the copper melts and evaporates under the action of the arc, and microcracks begin to form on the surface. The tungsten particles on the surface are re-sintered under the action of a high temperature, resulting in cracks in the tungsten skeleton. Under the action of high-temperature arcs, the gas pressure increases sharply, which forms compressive stress on the cracks formed by ablation and promotes the inward expansion of the cracks. At the same time, the repeated opening and closing of the contacts causes the copper at the front of the crack to melt, volatilize, expand, solidify, and shrink repeatedly, which also leads to crack propagation.
- (4) In the process of multiple opening and closing of the circuit breaker, melting and solidification occur alternately, and the middle part of the crack is continuously affected by the compression-tensile stress, which makes the crack propagate, and new cracks are generated in the process of the propagation, and the crack-like cracks are finally formed after repeated operations. The bulging and unevenness on the surface are aggravated, and the bulging is formed by the repeated vaporization and deposition of Cu in the alloy during the ablation process. There are trace amounts of Fe and Al in the energy



spectrum, which are mainly derived from the cast iron material of the contact base and a small amount of nozzle alumina filler.

- (5) The content of  $\text{CF}_4$  can not only be used to characterize the ablation discharge on the surface of the nozzle insulating material, but can also characterize the discharge decomposition degree of  $\text{SF}_6$  in the system by adding carbonaceous compounds. Through experiments, it is recommended that  $\text{CF}_4$  should reach  $600 \mu\text{l/l}$  as the threshold for judging whether the arc extinguishing chamber needs to be repaired. This method can be extended to the operating condition evaluation of arc extinguishing chamber of other types of the  $\text{SF}_6$  circuit breaker.

## AUTHOR DECLARATIONS

### Conflict of Interest

The authors have no conflicts to disclose.

## DATA AVAILABILITY

The data that support the findings of this study are available from the corresponding author upon reasonable request.

## REFERENCES

- <sup>1</sup>C. R. Heising, A. L. J. Janssen, W. Lanz *et al.*, "Summary of CIGRE 13.06 working group worldwide reliability data and maintenance cost data on high voltage circuit breakers above 63 kV," in *Proceedings of the 29th IAS Annual Meeting* (IEEE, Denver, 1994), pp. 2226–2234.
- <sup>2</sup>F. J. Sun, H. S. Qin, and Z. Q. Wang, "Diagnosis techniques on contact electrical endurance of high voltage circuit breakers," in *Proceedings of 1998 International Conference on Power System Technology* (IEEE, Beijing, China, 1998), pp. 105–109.
- <sup>3</sup>M. Landry, A. Mercier, G. Ouellet *et al.*, "A new measurement method of the dynamic contact resistance of HV circuit breakers," in *IEEE Power Engineering Society Transmission and Distribution Conference, PES TD 2005/2006* (IEEE, Dallas, 2006), pp. 1002–1009.
- <sup>4</sup>M. Landry, O. Turcotte, and F. Brikci, "A complete strategy for conducting dynamic contact resistance measurements on HV circuit breakers," *IEEE Trans. Power Delivery* **23**(2), 710–716 (2008).
- <sup>5</sup>Z. He, Z. Huang, Y. Zong, X. Cao, B. Xiang, X. Mao, Y. Zhang, and J. Kong, "Study on trigger lifetime of electrode on laser-triggered vacuum switch," *IEEE Trans. Plasma Sci.* **46**(10), 3683–3689 (2018).
- <sup>6</sup>X. Mao, Z. He, X. Xu *et al.*, "Research on the time delay characteristics of the laser triggered vacuum switch," *IEEE Trans. Plasma Sci.* **43**(6), 2005–2010 (2015).
- <sup>7</sup>Z. Huang, B. Xiang, X. Cao *et al.*, "Research on the pre-breakdown current of the laser-triggered vacuum switch," *IEEE Trans. Plasma Sci.* **46**(2), 410–414 (2018).
- <sup>8</sup>J. Tepper, M. Seeger, T. Votteler *et al.*, "Investigation on erosion of Cu/W contacts in high-voltage circuit breakers," *IEEE Trans. Compon. Packag. Technol.* **29**(3), 658–665 (2006).
- <sup>9</sup>X. Mao, Z. He, Y. Wang *et al.*, "Research on the interaction of primary plasma and main electrode for laser triggered vacuum switch," *IEEE Trans. Plasma Sci.* **42**(11), 3592–3597 (2014).